Robust Admittance Control for Human Arm Strength Augmentation With Guaranteed Passivity: A Complementary Design

Wulin Zou, Xiang Chen, *Member, IEEE*, Shilei Li, Pu Duan, Ningbo Yu, *Member, IEEE*, and Ling Shi, *Senior Member, IEEE*

***Abstract*—For the position-error feedback-based admittance control in human strength augmentation, there are inherent conflicts among different performances, such as accuracy, passivity, and robustness. In this article, we propose a multi-objective complementary control framework that enables decoupled nominal admittance performance and robustness while preserving the passivity. Essentially, the framework consists of three parts. An linear-quadratic-gaussian (LQG) controller and a feedforward controller, which jointly render the nominally accurate and passive admittance performance against noise, and a robust regulator, which recovers the nominal performance when disturbance and/or uncertainty exist. The efficacy of the proposed method is verified on a human arm strength augmentation device for load lifting. Compelling simulations, experiments, and comparison results demonstrate the efficacy and superiority of the proposed method.**

***Index Terms*—Admittance control, human strength augmentation, multi-objective complementary control, passivity.**

I. Introduction

HUMAN strength augmentation has been a promising research topic in the field of robotics and has attracted intensive research efforts in recent decades. Such a human-centered device serves to help human lifts up a heavy load with less effort. It includes some kinds of force augmentation exoskeleton robots [1]–[3], teleoperation robots [4], cooperation robots [5], [6], etc. The basic idea for strength augmentation is to reduce the apparent impedance (i.e., inertia, damping, and stiffness) felt by the human, which can be achieved by impedance compensation [1], admittance/impedance or shaping control [2], [3], [6], etc. Among them, admittance/impedance control is the most commonly used approach.

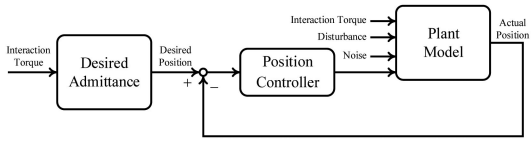

Fig. 1. General position-error feedback-based admittance control.

One substantial challenge in admittance control is the optimization/guarantee of multiple performance objectives. Rendering a desired admittance in a passive and accurate way is still challenging arising from many factors. First, the Bode gain-phase integral relationship reveals that there is inherent conflict between performance and passivity for the commonly used position-error feedback-based admittance control, as shown in Fig. 1 [7]. It is well-known that this kind of single-degree-of-freedom (DOF) framework cannot deal with multiobjective optimization problem effectively, since the requirements on the loop gain from different objectives (e.g., accuracy and robustness) cannot be fulfilled simultaneously [8]. Increasing the feedback gains can improve the accuracy significantly, however, at the cost of passivity in many cases. Second, practical experience shows that passivity can be easily violated when accurately rendering a virtual impedance, especially inertia, which is less than the physical one [9]. Third, disturbance/uncertainty incurs instability and degradation of fidelity [10]. Minimization of error, control effort, and disturbance and noise effects, along with guarantee of passivity, in one framework is beneficial, but still open. There have been a number of works on admittance control, but mostly focused on either the passivity-based design for safe interaction or robust control methods addressing disturbance and uncertainty.

For the passivity-based design, there are several ways, for example, by analyzing the stability and positive realness in

Manuscript received 16 October 2021; revised 13 March 2022 and 22 May 2022; accepted 7 July 2022. Recommended by Technical Editor Jinhua She and Senior Editor Hong Qiao. This work was supported in part by the National Natural Science Foundation of China under Grant U1913208, Grant 61873135, and Grant U1713223 and in part by Hong Kong ITF Fund under Grant GHP/001/18SZ. *(Corresponding author: Ningbo Yu.)*

Wulin Zou, Shilei Li, and Ling Shi are with the Department of Electronic and Computer Engineering, Hong Kong University of Science and Technology, Hong Kong, China (e-mail: wzouab@connect.ust.hk; slidk@connect.ust.hk; eesling@ust.hk).

Xiang Chen is with the Department of Electrical and Computer Engineering, University of Windsor, Windsor, ON N9B 3P4, Canada (e-mail: xchen@uwindsor.ca).

Pu Duan is with the Xeno Dynamics Company, Ltd., Shenzhen 518055, China (e-mail: duanpu@xeno.com).

Ningbo Yu is with the Institute of Robotics and Automatic Information Systems, and Tianjin Key Laboratory of Intelligent Robotics, Nankai University, Tianjin 300071, China (e-mail: nyu@nankai.edu.cn).

Color versions of one or more figures in this article are available at https://doi.org/10.1109/TMECH.2022.3191469.

Digital Object Identifier 10.1109/TMECH.2022.3191469

frequency-domain, or by using dissipativity in time-domain. With the stability and positive realness, the conditions and ranges regarding the controller gains and virtual admittance can be analyzed by symbolic calculation. These methods have been adopted in many existing works, for example, finding the constraints for admittance control [11]–[14], for admittance display of haptic and teleoperation devices [15]–[17], for cascaded proportional-integral-derivative (PID)-type impedance control of series elastic actuators [18]–[21], etc. It is straightforward, but nevertheless, it becomes extremely difficult when the order of the plant or controller is high. Aside from the frequency-domain methods, some researchers pursued passive interaction via time-domain approaches, such as the passivity observer-based methods [4], [22], [23], the energy tank-based methods [24], the Lyapunov function-based methods [25]–[27], and so on.

To improve the robustness against disturbance and model uncertainty, some robustification methods were proposed, including adaptive control [28], sliding-mode control [29], neural network-based control [30], etc. However, these methods did not consider passivity during the controller design.

Some researchers have been pursuing perfect admittance control (PAC) so that the system can achieve zero admittance error and passivity simultaneously under ideal modeling. In [12], natural admittance control (NAC) was proposed to achieve PAC via velocity and force feedback, which is different from the error-feedback controller. To achieve smaller desired impedance in real application, a mechanical filter with damper and spring is intentionally placed between the end-effector and the environment [31]. There are several issues for the NAC method. First, it can reject the Coulomb friction, but cannot attenuate other types of disturbance effectively, e.g., external load torque. Second, placing a mechanical filter will reduce the bandwidth of force control and may not be practical in many situations. Third, for some systems, the velocity cannot be directly measured, and how to address the process and measurement noises is also a question. Last, when the desired inertia is small, the force feedback gain can be very large, which may magnify the noise, and result in motor saturation and even instability.

Recently, a 2-DOF architecture (TDA)-based control was developed to decouple the design of the nominal perfect admittance shaping and disturbance rejection, which can circumvent the structural flaws of the conventional 1-DOF admittance control, as shown in Fig. 1 [32]. It was inspired by the well-known Youla–Kucera parameterization [33], [34], and designed to improve the robustness of the NAC method. The general law of the TDA method is a velocity and force feedback, which still requires the measurement of velocity and faces the challenge of large force feedback gain for small desired inertia case.

In this article, we propose a complementary design framework for admittance control in human arm strength augmentation, which results in the nonconservative design of accuracy, passivity, and robustness. First, we define the concept of PAC, where precisely zero error and passivity are achieved simultaneously under ideal modeling. Then, we propose a complementary design framework with a nominal full-information (FI) controller and a robust regulator, which decouples the regulation of admittance, performance, and robustness. We show that the nominal controller is able to achieve PAC for any passive virtual admittance under ideal modeling. Furthermore, it also estimates the unknown states and filters out the measurement and process noises. On the other hand, the robust regulator rejects the uncertain disturbance and recovers the nominal performance. To penalize the controller gains, we put certain norm constraints on the admittance error and control effort, and the gains are obtained by optimization. Finally, compelling simulations, experiments, and comparison results are presented to show the efficacy of the proposed method by using a robot arm for load handling. Compared with the existing literature, the main contributions of this article lie in the following aspects.

1) The proposed method decouples the design of admittance performance and robustness, which leads to a nonconservative and separate design for them.
2) The proposed nominal FI controller can achieve PAC with zero error and guaranteed passivity for a given ideal model.
3) The robust regulator works as an add-on to regulate the robustness against disturbance/uncertainty. It does not affect the nominal admittance performance when the disturbance is not present and will recover the performance when the system is disturbed.
4) Simulations, experiments, and comparison results show that the proposed method achieves precise admittance control and stable interaction with/without the unknown load and can reduce the subject's workload significantly.

Notations: Transpose of a matrix A is denoted as A^T, conjugate transpose is written as A^*, and $\|T(s)\|_2$ and $\|T(s)\|_\infty$ represent the $\mathcal{H}_2$ and $\mathcal{H}_\infty$ norms of transfer function $T(s)$, respectively. The sizes of all matrices and signals can be inferred from the context.

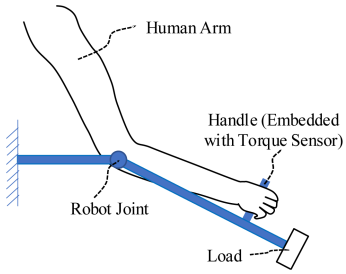

Fig. 2. Illustration of human arm strength augmentation. Human lifts up a heavy load assisted by a robot.

II. Problem Statement

A. System Modeling

Without loss of generality, a robot arm for human strength augmentation is shown in Fig. 2. The model is written as

$$m_1\ddot{\theta} + m_2\ddot{\theta} + b\dot{\theta} + (\tilde{m}_1 l_1 + \tilde{m}_2 l_2)g\sin\theta = u + \tau + \tau_f \quad (1)$$

where m_1 and b are the mechanical inertia and damping of the robot itself, respectively, m_2 is the inertia of the added load, $\tilde{m}_1$ and $\tilde{m}_2$ are the masses of the robot link and load, respectively,

l_1 and l_2 denote the centers of mass, g is the gravitational acceleration, θ is the rotation angle of the joint, u is the command, τ is the interaction torque between the human and robot, and τ_f is other unmodeled dynamics, including nonlinear frictions and other model uncertainties.

Here, we linearize the link gravitational term $\tilde{m}_1 g l_1 \sin\theta$ at the origin, such that

$$\tilde{m}_1 g l_1 \sin\theta = k\theta + \mathcal{O}(\theta) \tag{2}$$

where $k = \tilde{m}_1 g l_1$ and $\mathcal{O}(\theta)$ is the high-order residual term. For load-lifting tasks, the external load (i.e., m_2 and $\tilde{m}_2$) is unknown. The added load torque and other unmodeled dynamics can be grouped as a lumped disturbance since they need to be rejected. Let

$$d = \tau_f - m_2\ddot{\theta} - \tilde{m}_2 g l_2 \sin\theta - \mathcal{O}(\theta) \tag{3}$$

where d is the lumped disturbance with the assumption of bounded amplitude. Therefore, the original model in (1) can be rewritten by a disturbed linear model, i.e.,

$$m\ddot{\theta} + b\dot{\theta} + k\theta = u + \tau + d \tag{4}$$

where $m = m_1$. Here, we assume that only the position can be measured directly.

Taking into consideration the measurement and process noises, the state-space representation of the linearized model can be written as

$$\begin{cases} \dot{x} = Ax + B_0 w_0 + B_1 w_1 + B_2 w_2 + B_3 u \\ y = C_3 x + D_{30} w_0 \end{cases} \tag{5}$$

where $w_0 \in \mathbb{R}^{2\times 1}$ is a white Gaussian noise signal, $w_1 = d \in \mathbb{R}$, $w_2 = \tau \in \mathbb{R}$, $y \in \mathbb{R}$ is the measured position of the robot, $x = [\theta\ \dot{\theta}]^T \in \mathbb{R}^{2\times 1}$ is the state, and

$$A = \begin{bmatrix} 0 & 1 \\ -\dfrac{k}{m} & -\dfrac{b}{m} \end{bmatrix}, B_1 = \begin{bmatrix} 0 \\ \dfrac{1}{m} \end{bmatrix}, B_2 = \begin{bmatrix} 0 \\ \dfrac{1}{m} \end{bmatrix}$$

$$B_3 = \begin{bmatrix} 0 \\ \dfrac{1}{m} \end{bmatrix}, C_3 = \begin{bmatrix} 1\ 0 \end{bmatrix}. \tag{6}$$

Matrices B_0 and D_{30} are the weighting matrices for the noise.

The admittance model is defined by the dynamical relationships between the interaction torque and output position/velocity, i.e.,

$$Z_1(s) = \frac{\theta(s)}{\tau(s)}, Z_2(s) = \frac{\dot{\theta}(s)}{\tau(s)} = sZ_1(s). \tag{7}$$

B. Admittance Shaping at the Interactive Port

If the admittance at the interactive port is augmented, the subject will feel easy to push the robot with less effort. It can be realized by admittance control by setting the desired parameters to respective levels. The desired admittance model is given by

$$Z_{1d}(s) = \frac{\theta_d(s)}{\tau(s)} = \frac{1}{m_d s^2 + b_d s + k_d}, Z_{2d}(s) = sZ_{1d}(s) \tag{8}$$

where $m_d > 0, b_d > 0$, and $k_d > 0$ are the desired inertia, damping, and stiffness, respectively, and θ_d is the desired position.

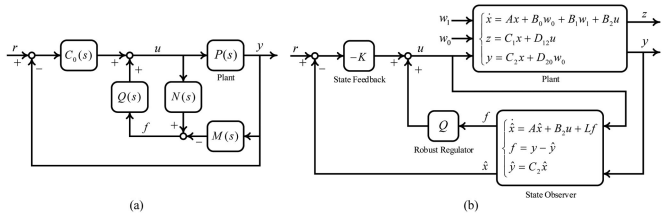

Fig. 3. Diagram of the complementary control. (a) Framework developed in [35], which is originated from the Youla–Kucera parameterization [33], [34], [37]. (b) One special state-space realization using the linear-quadratic-gaussian (LQG) control [36].

Without loss of generality, $m_d \neq m, b_d \neq b$, and $k_d \neq k$ are assumed. The state-space representation is given by

$$\begin{cases} \dot{x}_d = A_d x_d + B_d w_2 \\ y_d = C_d x_d \end{cases} \tag{9}$$

where $x_d = [\theta_d\ \dot{\theta}_d]^T \in \mathbb{R}^{2\times 1}$ is the desired state, $y_d \in \mathbb{R}$ is the desired position, and

$$A_d = \begin{bmatrix} 0 & 1 \\ -\dfrac{k_d}{m_d} & -\dfrac{b_d}{m_d} \end{bmatrix}, B_d = \begin{bmatrix} 0 \\ \dfrac{1}{m_d} \end{bmatrix}, C_d = \begin{bmatrix} 1\ 0 \end{bmatrix}. \tag{10}$$

The position error

$$e = y_d - y \tag{11}$$

can be used to characterize the admittance rendering error.

C. Perfect Admittance Control

Here, we define the concept of "perfect" admittance control under ideal modeling without disturbance/uncertainty.

Definition 1 (PAC): Suppose the noise $w_0 = 0$ and disturbance $w_1 = 0$, given a passive desired admittance model in (8) with $m_d \neq m, b_d \neq b$, and $k_d \neq k$, PAC is to find a control action u such that the following two are satisfied simultaneously.

a) The error between the desired admittance $Z_{1d}(s)$ and the closed-loop admittance $\bar{Z}_1(s)$ is exactly zero, i.e., $E_Z(s) = Z_{1d}(s) - \bar{Z}_1(s) = 0$.

b) The closed-loop admittance $\bar{Z}_2(s) = s\bar{Z}_1(s)$ is passive.

In the following section, we will show how to arrive at PAC theoretically, and then address the noise and disturbance.

III. Complementary Design of Admittance Control

A. Multi-objective Complementary Control

The framework of complementary control is shown in Fig. 3, which was developed in [35] and [36], where $C_0(s)$ is a stabilizing controller for the nominal plant $P(s) = M^{-1}(s)N(s)$ with $M(s)$ and $N(s)$ given as the left co-prime factorizations of $P(s)$, $Q(s)$ is an arbitrary stable transfer function, $\hat{x}$ and $\hat{y}$ are the observed state and output, respectively, r is the reference signal, K and L are the state feedback and observer gains, respectively, and the plant $P(s)$ takes a general state-space representation.

Apparently, $f = N(s)u - M(s)y$ denotes the residual error between the actual sensor output and the observer output. Hence,

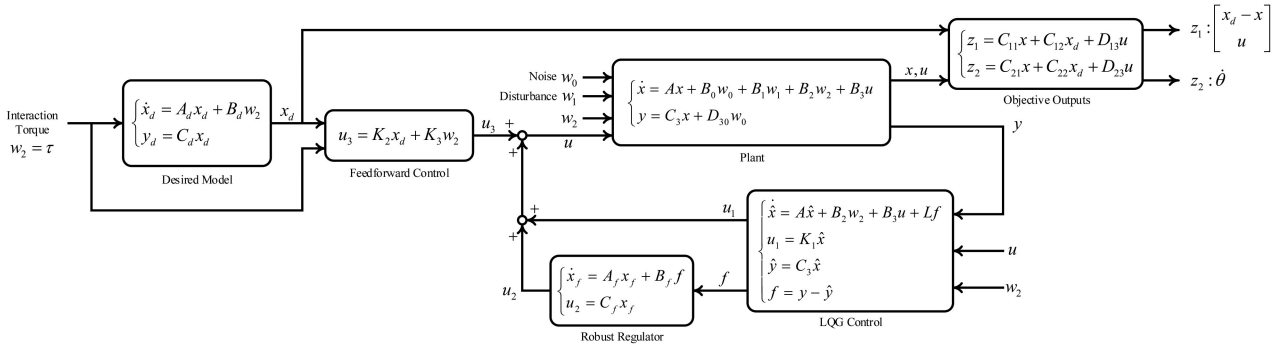

Fig. 4. Proposed framework for admittance control for human strength augmentation. The LQG and feedforward controller jointly render the nominal admittance performance with guaranteed passivity, and the robust regulator recovers the nominal performance when disturbance and/or uncertainty exist.

$Q(s)$, which is driven by f, can be designed to regulate the robustness against the uncertain disturbance. Fig. 3(b) shows a feasible realization of the complementary control, where the nominal controller $C_0(s)$ is designed as an LQG controller. When the nominal plant is not subject to disturbance, the performance will be the nominal one achieved by $C_0(s)$ since f is zero. When disturbance is present, $Q(s)$ will be activated to reduce the impact of disturbance on the output and recover the nominal performance. This framework provides a way to decouple the regulation on tracking and robustness, since the nominal controller $C_0(s)$ and robust regulator $Q(s)$ can be designed separately.

B. Proposed Complementary Admittance Control

Motivated by Fig. 3, the proposed structure for human strength augmentation is presented in Fig. 4. The control input u contains three parts: 1) u_1 from the LQG; 2) u_2 from the robust regulator; and 3) u_3 from the feedforward control. The robust regulator $Q(s)$ is represented by a state-space representation. Gains $K_1 \in \mathbb{R}^{1\times 2}$, $K_2 \in \mathbb{R}^{1\times 2}$, $K_3 \in \mathbb{R}$, $L \in \mathbb{R}^{2\times 1}$, $A_f \in \mathbb{R}^{n_f \times n_f}$, $B_f \in \mathbb{R}^{n_f \times 1}$, and $C_f \in \mathbb{R}^{1\times n_f}$ are the gain matrices to be determined, n_f is the order of the regulator, $x_f \in \mathbb{R}^{n_f \times 1}$ is the state of the regulator, and $\hat{x} \in \mathbb{R}^{2\times 1}$ is the state of the observer.

Remark 1: The output $z_1 = C_{11}x + C_{12}x_d + D_{13}u$, where $C_{11} = -C_{12}$ and D_{13} is a weight for u, i.e., $z_1 = C_{12}(x_d - x) + D_{13}u$, is used to minimize the admittance error and penalize the control effort. The output $z_2 = C_{21}x + C_{22}x_d + D_{23}u$, where $C_{21} = [0\ 1], C_{22} = [0\ 0]$, and $D_{23} = 0$, i.e., $z_2 = \dot{\theta}$, is defined for passivity so that the closed-loop admittance $\bar{Z}_2(s) = \bar{T}_{z_2 w_2}(s) = \bar{T}_{\dot{\theta}\tau}(s)$ is passive.

Remark 2: Though both the proposed and the TDA methods [32] are originated from the Youla–Kucera parameterization, they have different structures intrinsically. The TDA controller consists of a force feedback and a velocity feedback, while our method has three parts: 1) an LQG controller; 2) a feedforward controller; and 3) a robust regulator.

The relationship between the proposed control shown in Fig. 4 and the complementary control shown in Fig. 3 is apparent. When $w_2 = 0$ and $r = 0$, Fig. 4 becomes exactly the one in Fig. 3(b). When $w_0 = 0$ and $w_1 = 0$, the state observer will precisely estimate the actual state with zero error, i.e., $f = 0$ and $\hat{x} = x$, indicating that $u_2 = 0$ and $u = u_1 + u_3 = K_1 x + K_2 x_d + K_3 w_2$. Hence, the nominal controller for the proposed framework in Fig. 4 is an FI feedback controller. With the same trick, it is easy to show that the transfer relationships from u_3 and w_2 to y, z_1, and z_2 are independent on the robust regulator $Q(s)$ and observer gain L. Hence, the passivity of the closed-loop admittance function $\bar{Z}_2(s)$ from τ to $\dot{\theta}$ is also independent on the robust regulator $Q(s)$ and observer gain L. Some benefits of the proposed framework are summarized as follows:

1) The FI controller $u = K_1 x + K_2 x_d + K_3 w_2$ works as the nominal controller, which is able to achieve PAC such that the closed-loop admittance function is passive and admittance error is zero for a given ideal model.
2) When the system has no disturbance, the performance is dominated by the nominal controller. Otherwise, the robust regulator $Q(s)$ rejects the disturbance and recovers the nominal performance.
3) The LQG control improves the response, observes the unknown states, and filters out the noises.

C. PAC by the FI Feedback Controller

The diagram of the nominal FI control is shown in Fig. 5, where the feedback law can be explicitly written as

$$u = \bar{k}_1\theta + \bar{k}_2\dot{\theta} + \bar{k}_3\theta_d + \bar{k}_4\dot{\theta}_d + \bar{k}_5\tau \tag{12}$$

where $K_1 = [\bar{k}_1\ \bar{k}_2]$, $K_2 = [\bar{k}_3\ \bar{k}_4]$, and $K_3 = \bar{k}_5$.

Proposition 1: There exist an infinite number of gain pairs $(\bar{k}_1, \bar{k}_2, \bar{k}_3, \bar{k}_4, \bar{k}_5)$ satisfying

$$\begin{cases} \bar{k}_5 m_d + m_d = m \\ \bar{k}_5 b_d + b_d + \bar{k}_4 = b - \bar{k}_2 \\ \bar{k}_5 k_d + k_d + \bar{k}_3 = k - \bar{k}_1 \\ b - \bar{k}_2 > 0, k - \bar{k}_1 > 0 \end{cases} \tag{13}$$

such that the FI controller (12) achieves PAC for any given passive admittance (8).

Proof: The closed-loop admittance for (12) is derived as

$$\bar{Z}_1(s) = Z_{1d}(s)\bar{Z}_{1r}(s) \tag{14}$$

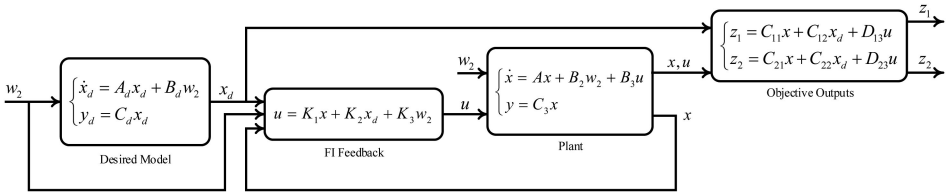

Fig. 5. Nominal admittance control with the FI feedback.

where

$$\bar{Z}_{1r}(s) = \frac{(\bar{k}_5 m_d + m_d)s^2 + (\bar{k}_5 b_d + b_d + \bar{k}_4)s + \bar{k}_5 k_d + k_d + \bar{k}_3}{ms^2 + (b - \bar{k}_2)s + k - \bar{k}_1}.$$

As one can see, $\bar{Z}_1(s) = Z_{1d}(s)$ is obtained when

$$\begin{cases} \bar{k}_5 m_d + m_d = m \\ \bar{k}_5 b_d + b_d + \bar{k}_4 = b - \bar{k}_2 \\ \bar{k}_5 k_d + k_d + \bar{k}_3 = k - \bar{k}_1 \end{cases}. \tag{15}$$

Noted that $Z_{2d}(s) = sZ_{1d}(s)$ is passive, to be passive for $\bar{Z}_2(s) = s\bar{Z}_1(s)$, $Z_{1r}(s)$ should have no unstable pole-zero cancellation, which requires

$$b - \bar{k}_2 > 0, k - \bar{k}_1 > 0. \tag{16}$$

It shows that $\bar{k}_5$ is determined by $\bar{k}_5 = \frac{m - m_d}{m_d}$, while $\bar{k}_1, \bar{k}_2, \bar{k}_3$, and $\bar{k}_4$ are determined by the inequalities (16) and the two surfaces $\bar{k}_1 + \bar{k}_3 = k - k_d - \bar{k}_5 k_d$ and $\bar{k}_2 + \bar{k}_4 = b - b_d - \bar{k}_5 b_d$. Given any passive desired admittance, one can find an infinite number of gain pairs $(\bar{k}_1, \bar{k}_2, \bar{k}_3, \bar{k}_4, \bar{k}_5)$ such that the nominal FI controller achieves PAC.

Remark 3: Control laws with partial state feedback, e.g., $u = \bar{k}_1\theta + \bar{k}_2\dot{\theta} + \bar{k}_5\tau$, $u = \bar{k}_3\theta_d + \bar{k}_4\dot{\theta}_d + \bar{k}_5\tau$, $u = \bar{k}_1\theta + \bar{k}_4\dot{\theta}_d + \bar{k}_5\tau$, and $u = \bar{k}_2\dot{\theta} + \bar{k}_3\theta_d + \bar{k}_5\tau$, can also achieve PAC. However, they are special cases of the FI feedback.

Remark 4: Let $K_1 = -K_2$ and $K_3 = 0$, the nominal FI controller degenerates to a proportional-derivative (PD)-like controller. However, PAC is no longer retained, since (13) does not hold anymore.

D. Nominal Performance Recovery by the Robust Regulator

The nominal controller is sensitive to disturbance. Thanks to the complementary control framework, the design of the nominal performance and robustness can be decoupled without potential tradeoff. The robust regulator is designed as

$$\begin{cases} \dot{x}_f = A_f x_f + B_f f \\ u_2 = C_f x_f \end{cases} \tag{17}$$

which is to reduce the effect of disturbance on the objective output z_1. It can be synthesized, for example, using the $\mathcal{H}_\infty$ technique.

IV. Controller Synthesis

A. LQG Controller

In Fig. 4, suppose $w_1 = 0$, $w_2 = 0$, $D_{13}^T D_{13} > 0$, and $D_{30} D_{30}^T > 0$, we obtain a simplified diagram shown in Fig. 6.

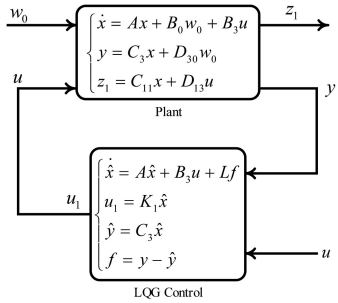

Fig. 6. Simplified diagram for the design of the LQG controller.

The LQG controller with gain matrices K_1 and L is designed such that the $\mathcal{H}_2$ norm of the transfer function from the noise w_0 to the output z_1 is minimized, i.e.,

$$\min_{K_1, L} \|T_{z_1 w_0}(s)\|_2. \tag{18}$$

The resulted minimal $\mathcal{H}_2$ cost is denoted by μ_1.

B. Feedforward Controller With Guaranteed Passivity and Admittance Performance

For the nominal controller shown in Fig. 5, the remaining parameters to be determined are K_2 and K_3 in the feedforward controller. Since K_1 is already obtained from the LQG control, the other two gains K_2 and K_3 can be calculated by the PAC condition in (13). However, the following remark shows that we need to optimize the controller gains.

Remark 5: Though PAC can be achieved by (13), it is not desirable in some cases, e.g., when m_d is very small. As shown by (13), $\bar{k}_5$ will be extremely large if m_d approaches to zero, which can magnify the noise in the measured torque and even cause saturation and instability. Hence, we need to optimize the gains so that the control signal does not exceed the saturation limit too much, which is at the cost of PAC.

Hence, for the diagram shown in Fig. 5, we include the control effort into the objective output z_1 to penalize it, and propose to find the gains by solving the following optimization problem:

$$\begin{aligned} &\min_{K_2, K_3} \|T_{z_1 w_2}(s)\|_\infty \\ &\text{s.t. } T_{z_2 w_2}(j\omega) + T_{z_2 w_2}^*(j\omega) \geq 0 \end{aligned} \tag{19}$$

where the second formula is to guarantee passivity, while the first is to optimize the admittance error and control effort. The resulted minimal $\mathcal{H}_\infty$ cost is denoted by γ_1.

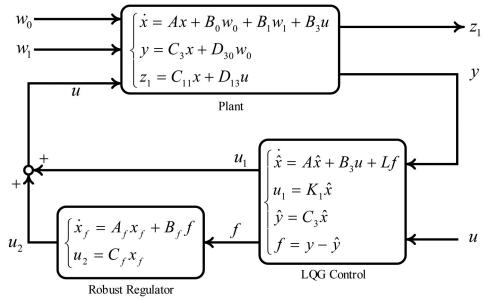

Fig. 7. Simplified diagram for the design of the robust regulator.

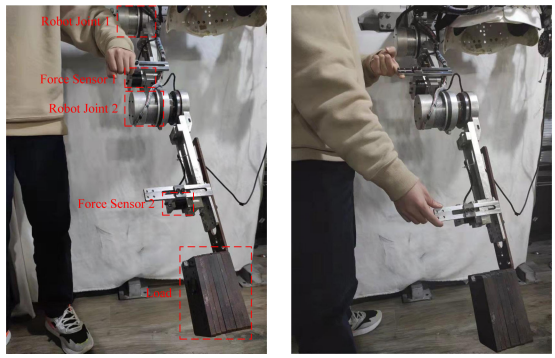

Fig. 8. Experimental setups. Left-hand side: 1-DOF configuration where the second joint is locked. Right-hand side: 2-DOF configuration where the second joint is free to move.

Remark 6: Though we penalize the control effort, the controller gains obtained by (19) can be very close to that obtained by the PAC (13) in many cases, e.g., large impedance case. Moreover, let $D_{13} = 0$, i.e., no penalty on the control effort, the optimal solution obtained by (19) is equivalent to that obtained by (13), i.e., PAC is recovered.

C. Reduced-Order Robust Regulator

In Fig. 4, let $w_2 = 0$, we obtain a simplified diagram, as shown in Fig. 7. It should be noted that a full-order robust regulator may be difficult to realize in a real platform. Hence, a reduced-order form is designed here. The order n_f will be specified during controller synthesis. The objective is to find the gain matrices A_f, B_f, and C_f, such that

$$\|T_{z_1w_1}(s)\|_\infty < \gamma_2 \text{ and } \min \left\|\tilde{T}_{z_1w_0}(s)\right\|_2 \tag{20}$$

for the closed-loop system shown in Fig. 7, where $\gamma_2 > 0$ is a given performance index, which guarantees that the maximum singular value of the frequency response from the disturbance w_1 to the output z_1 is less than γ_2. The resulted minimal $\mathcal{H}_2$ cost for the noise function $\tilde{T}_{z_1w_0}(s)$ is denoted by μ_2.

D. Analysis of the Closed-Loop Performance

Though the three units in our method are designed step by step, the closed-loop admittance performance, robustness, and stability can be guaranteed for the diagram shown in Fig. 4. Here, we denote the final closed-loop transfer function by $\bar{T}(s)$.

When considering the admittance performance, which is characterized by the transfer functions $\bar{T}_{z_1w_2}(s)$ and $\bar{T}_{z_2w_2}(s)$, let $w_0 = 0$ and $w_1 = 0$, one can show that the diagram in Fig. 4 can be simplified to be the one shown in Fig. 5. If the optimization problem in (19) has a solution, we conclude that the closed-loop admittance $\bar{T}_{z_2w_2}(s)$ is passive and $\|\bar{T}_{z_1w_2}(s)\|_\infty$ is bounded by γ_1 for the diagram shown in Fig. 4. Similarly, when considering the robustness against disturbance, let $w_0 = 0$ and $w_2 = 0$, the diagram shown in Fig. 4 can be simplified to be the one shown in Fig. 7. If the optimization problem in (20) has a solution, the disturbance effect on the output, i.e., $\|\bar{T}_{z_1w_1}(s)\|_\infty$ shown in Fig. 4, will be bounded by γ_2.

Theorem 1: The closed-loop system shown in Fig. 4 is internally stable if K_1 and L are obtained by the LQG, the desired admittance is passive, and the robust regulator is designed by satisfying the $\mathcal{H}_\infty$ constraint in (20).

Proof: Let $\bar{x} = [x^T\ x_d^T\ x_f^T\ e_x^T]^T$, where $e_x = x - \hat{x}$, one can obtain the closed-loop dynamics of the states, i.e.,

$$\dot{\bar{x}} = \bar{A}\bar{x} + \bar{B}_0w_0 + \bar{B}_1w_1 + \bar{B}_2w_2 \tag{21}$$

where

$$\bar{A} = \begin{bmatrix} A + B_3K_1 & B_3K_2 & B_3C_f & -B_3K_1 \\ 0 & A_d & 0 & 0 \\ 0 & 0 & A_f & B_fC_3 \\ 0 & 0 & 0 & A - LC_3 \end{bmatrix}. \tag{22}$$

Matrices $\bar{B}_0$, $\bar{B}_1$, and $\bar{B}_2$ are not of interest. Since the LQG is stabilizing, $A + B_3K_1$ and $A - LC_3$ are Hurwitz. Matrix A_d is Hurwitz because the desired admittance is a passive function. Matrix A_f is Hurwitz if the $\mathcal{H}_\infty$ constraint in (20) is satisfied. This means that $\bar{A}$ is Hurwitz. Hence, we can conclude that the internal stability is ensured by the proposed method. The proof is complete.

V. Simulation and Experimental Results

A. Experimental Setup for Human Arm Strength Augmentation

The platform for experiments is shown in Fig. 8. The human can drive the robot joint rotate around the joint center from the vertical to the horizontal position, while the robot helps to lift up the heavy load. There are two force sensors mounted on the links to measure the equivalent interactive torques and there is a heavy load on the end. The joint positions are measured by encoders, while the velocities need to be estimated. The experiments are conducted via MATLAB/Simulink Real-Time with a control frequency of 1 kHz. Optimization problems in (18)–(20) are solved by MATLAB function *systune* using the nonsmooth optimization [38]. Each optimization problem can be solved in less than 5 s on a desktop computer (Windows 7, Intel i5-4460, quad-core CPU, 4 GB RAM, MATLAB 2017B).

The main parameters of the platform are given in Table I, and the two joints take the same parameters. Other matrices for

TABLE I
MAIN PARAMETERS OF THE PLATFORM FOR EACH JOINT

Parameter	Value
Inertia m (N·m · s^2/rad)	1.2
Damping b (N·m · s/rad)	7.232
Stiffness k (N·m/rad)	10.0
Reduction ratio	80
Motor nominal torque (N·m)	75
Load (kg)	8.8
Location of the load l_2 (m)	0.91

controller synthesis are given as

$$B_0 = \begin{bmatrix} 0 & 0 \\ 0 & 0.001 \end{bmatrix}, D_{30} = \begin{bmatrix} 10^{-6} & 0 \end{bmatrix}, C_{11} = \begin{bmatrix} 1000 & 0 \\ 0 & 10 \\ 0 & 0 \end{bmatrix}$$

$$C_{12} = -C_{11}, D_{13} = \begin{bmatrix} 0 \\ 0 \\ 1 \end{bmatrix}, C_{21} = \begin{bmatrix} 0 & 1 \end{bmatrix}, C_{22} = \begin{bmatrix} 0 & 0 \end{bmatrix}$$

$$D_{23} = 0, \gamma_2 = 1.2, n_f = 3. \quad (23)$$

With the given parameters, by solving the optimization problem in (18), the LQG controller can be obtained with $K_1 = [-966.6743 \ -42.4026]$ and $L = [39.3831 \ 778.6601]^T$. By solving the optimization problem (20), the matrices of the robust regulator are obtained as

$$A_f = \begin{bmatrix} -348.7 & 47.6 & 119.6 \\ -151.9 & 12.1 & 259.8 \\ -532.0 & 32.9 & 65.0 \end{bmatrix}, \ B_f = \begin{bmatrix} -4643.4 \\ -3204.9 \\ -6373.7 \end{bmatrix}$$

$$C_f = \begin{bmatrix} 394.3 & 77.6 & 215.1 \end{bmatrix}. \quad (24)$$

The resulted $\mathcal{H}_2$ costs are $\mu_1 = 0.0148$ and $\mu_2 = 0.1893$, respectively. The matrices K_1, L, A_f, B_f, and C_f will be maintained for different cases, since they are only associated with the open-loop plant, while the remaining gains K_2 and K_3 will be determined after given the desired admittance.

B. Simulation Results

1) Nominal Admittance Performance With the FI Feedback Controller: For the nominal controller shown in Fig. 5, when $m_d = 0.2m$, $b_d = 0.2b$, and $k_d = 0.2k$, the gains obtained from (13) and (19) are $K_2 = [966.6743 \ \ 42.4026], K_3 = 4.0000$ and $K_2 = [966.5966 \ \ 42.3581], K_3 = 3.9998$, respectively. They are almost the same since the objective output z_1 puts less penalty on the control effort in this case. Another example, if we set $m_d = 0.1m$, $b_d = 0.5b$, and $k_d = 0.5k$, the gains obtained from (13) and (19) are $K_2 = [926.6743 \ \ 13.4746], K_3 = 9.0000$ and $K_2 = [918.6723 \ \ 13.8093]$, and $K_3 = 5.4040$, respectively. We can see that the gain K_3 is reduced significantly since the objective output z_1 gives more penalty on u in this situation.

The bode plots of the closed-loop admittance are shown in Fig. 9(a). The passivities of all cases are guaranteed since the phases are in the range of $[-90^\circ \ 90^\circ]$ over the full frequency range. In case 1, the closed-loop admittance of the proposed method matches exactly with the desired admittance and the one obtained by PAC. In case 2, the optimized closed-loop admittance is very close to the desired in the low-frequency range (i.e., 0–3 Hz), but deviates from it in the high-frequency range. In Fig. 9(b), the singular values of the closed-loop function $\bar{T}_{uw_2}(s)$ for the PAC case and the optimized case are presented. For the PAC case, a small interaction torque w_2 can result in a large control effort due to the large gain K_3, which should be avoided, since there are noises in the torque sensor in experiments. In contrast, the optimized case can significantly reduce the control effort over the full frequency range.

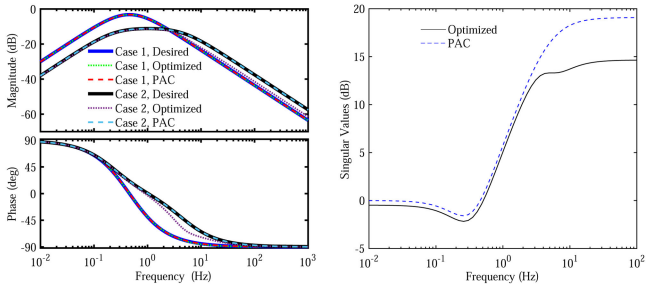

Fig. 9. (a) Bode plots of the closed-loop admittance functions $\bar{Z}_2(s)$. Case 1: $m_d = 0.2m$, $b_d = 0.2b$, and $k_d = 0.2k$. Case 2: $m_d = 0.1m$, $b_d = 0.5b$, and $k_d = 0.5k$. Desired: Desired admittance $\frac{s}{m_d s^2 + b_d s + k_d}$. Optimized: Resulted closed-loop admittance when the gains are obtained by solving (19). PAC: Resulted admittance by solving (13). (b) Singular values of the closed-loop function $\bar{T}_{uw_2}(s)$ when $m_d = 0.1m$, $b_d = 0.5b$, and $k_d = 0.5k$.

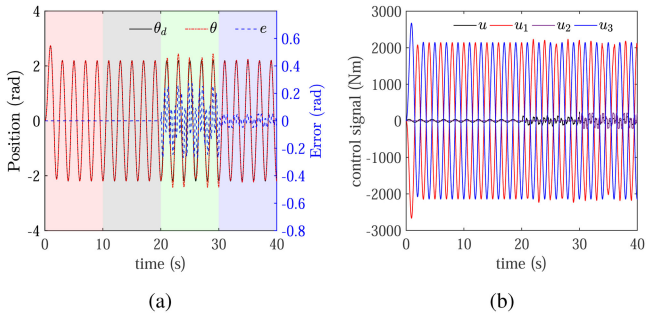

Fig. 10. Simulation results of the proposed admittance control under different situations for $m_d = 0.2m$, $b_d = 0.2b$, and $k_d = 0.2k$. Four shaded areas indicate the nominal controller $u = u_1 + u_3$ without disturbance (0–10 s), the nominal controller with the robust regulator $u = u_1 + u_2 + u_3$ without disturbance (10–20 s), the nominal controller under disturbance (20–30 s), and the nominal controller with the robust regulator under disturbance (30–40 s), respectively. (a) Desired position, the actual position, and the position error. (b) Control signal.

2) Recovery of the Nominal Performance With the Robust Regulator: The simulations are conducted under four conditions, as shown in Fig. 10. The interactive torque w_2 is given as $10\sin(\pi t)$ N·m. The disturbance w_1 is set as the sum of a step signal (amplitude: -50 N·m), a cyclic pulse signal (amplitude: 100 N·m, period: 0.6 s, and pulse width: 0.3 s), and a sinusoidal gravitational signal ($30\sin\theta$ N·m). The noise takes unit power density for each entry. With the robust regulator to reject disturbance, the admittance error under disturbance are

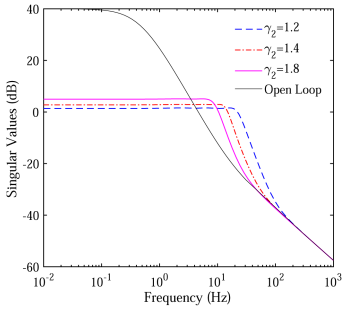

Fig. 11. Singular values of the closed-loop disturbance function $\bar{T}_{z_1 w_1}(s)$.

reduced significantly. The additional robust regulator does not affect the nominal performance when disturbance is not present; instead it recovers the nominal performance under disturbance.

The singular values of the closed-loop disturbance function $\bar{T}_{z_1 w_1}(s)$ are shown in Fig. 11, which denotes the disturbance effect on the objective output. As one can see, compared with the open-loop case (maximum singular value: 40 dB, i.e., 100 in absolute value), the maximum singular value is reduced remarkably for the proposed method (maximum singular value: 1.5 dB, i.e., 1.19 in absolute value). Besides, reducing the given bound, γ_2, also brings down the maximum singular value.

C. Experimental Results

In this section, we present the comparison results of four different methods and the results of workload reduction on the platform with 1-DOF configuration, and also provide the results on the platform with 2-DOF configuration. During the comparison, the desired admittances for the four methods are all set as $m_d = 0.2m$, $b_d = 0.2b$, and $k_d = 0.2k$.

1) Comparison With the NAC: The natural admittance controller is given by [9]

$$u = G_f \tau - G_v \dot{\theta}. \tag{25}$$

Since the actual velocity $\dot{\theta}$ is unknown in our application, instead we implement the natural admittance controller as

$$u = G_f \tau - G_v s\theta. \tag{26}$$

The gain function G_v is usually chosen to be a constant. To achieve perfect admittance matching, G_f is designed as

$$G_f = G_v Z_{2d}(s) + \frac{Z_{2d}(s)}{Z_{2o}(s)} - 1 \tag{27}$$

where $Z_{2o}(s) = \frac{s}{ms^2+bs+k}$ is the open-loop admittance and $Z_{2d}(s) = \frac{s}{m_d s^2+b_d s+k_d}$ is the desired admittance.

During the experiment, G_v is set to be 70 to have enough bandwidth. The results are shown in Fig. 12(a), which show a relatively large admittance error (maximum error: 0.3118 rad). Due to the heavy load on the end-effector, there is a biased error between the actual and desired positions, which cannot be diminished due to the limited robustness of the NAC method. Compared with the results of the proposed method in Fig. 12(d), the maximum error of the NAC method is about 9.3-times larger than that of the proposed method (maximum error: 0.0302 rad). In addition, the control signal of the NAC method is much noisy, which is caused by the derivative of position. It should be noted that we also try to use a filter to smooth it, which, however, no longer promises the passivity of the closed-loop admittance.

2) Comparison With the TDA-Based Method: The TDA-based controller is designed as [32]

$$u = [(1 + G_v Z_{2o})G_f + G_v Z_{2o}]\,\tau - G_v \dot{\theta}. \tag{28}$$

Similar to the NAC method, the velocity $\dot{\theta}$ is replaced by $s\theta$ as

$$u = [(1 + G_v Z_{2o})G_f + G_v Z_{2o}]\,\tau - G_v s\theta \tag{29}$$

where $G_f = \dfrac{Z_{2d}(s)}{Z_{2o}(s)} - 1$, $G_v = \dfrac{g_v}{sZ_{2o}(s)}$, and $g_v > 0$ is a constant to tune the bandwidth.

Taking $g_v = 70$, the experimental results are obtained, as shown in Fig. 12(b). The maximum admittance error is about 0.0454 rad, slightly larger than that of the proposed method. Though the error can be reduced by increasing g_v, the noise in the control signal needs careful treatment, which can result in instability if the noise is large. In contrast, our method achieves smoother control signal, since we use the LQG to estimate the unknown states and filter out the measurement and process noises.

3) Comparison With the Disturbance Observer-Based Method: Here, we take the extended state observer (ESO)-based controller [39] for comparison, which has a very similar structure as the proposed method in Fig. 4, but with the LQG and robust regulator replaced by an ESO and a disturbance compensator, respectively. The ESO uses the following formula to estimate the state and disturbance:

$$\begin{cases} \dot{\hat{x}} = A\hat{x} + B_1\hat{w}_1 + B_2 w_2 + B_3 u + L_x(y - \hat{y}) \\ \dot{\hat{w}}_1 = L_w(y - \hat{y}) \\ \hat{y} = C_3\hat{x} \end{cases} \tag{30}$$

where $\hat{w}_1$ is the estimated disturbance. The ESO-based controller is designed to be

$$u = u_1 + u_2 + u_3 \tag{31}$$

where $u_1 = K_1\hat{x}$ and $u_3 = K_2 x_d + K_3 w_2$. Since $B_1 = B_2$, u_2 needs to be $u_2 = -\hat{w}_1$ for disturbance compensation.

In the experiment, K_1, K_2, and K_3 are the same as the proposed method, while the observer gain $L_x = [370.96\ 4.51 \times 10^4]^T$ and $L_w = 2.38 \times 10^6$ are obtained such that the poles of the error dynamics of the ESO all locate at -40π. Hence, the observer has a bandwidth of about 20 Hz, which should be enough for admittance control. The maximum admittance error is about 0.0496 rad, also larger than the proposed method. Besides, the control signal of the ESO method shows relatively severe oscillations during experiment, as shown in Fig. 12(c). After analyzing the control signal, we find that this kind of oscillations are mainly caused by the inappropriate assumption of the disturbance estimation model [i.e., $\dot{\hat{w}} = L_w(y - \hat{y})$]. In the experiment, the disturbance, which

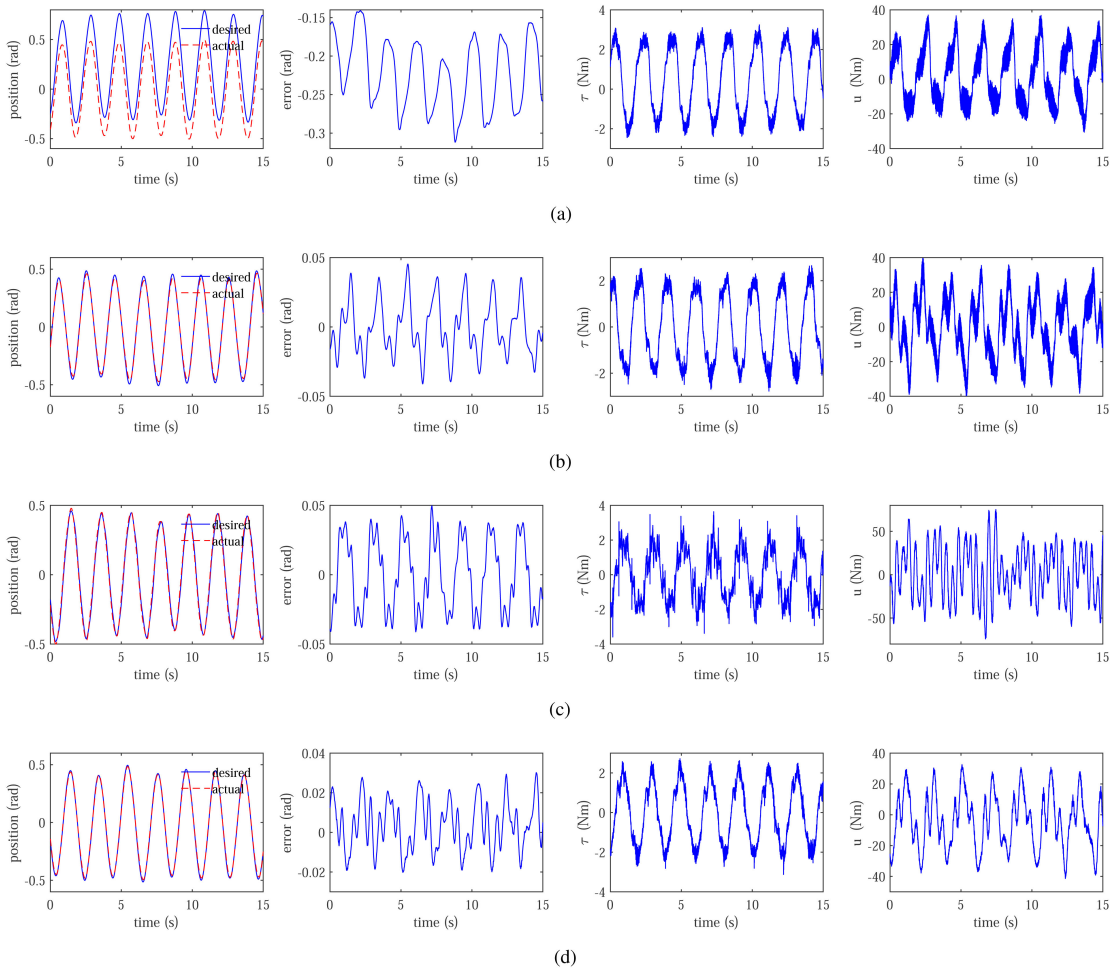

Fig. 12. Experimental results for different methods when $m_d = 0.2m$, $b_d = 0.2b$, and $k_d = 0.2k$ on the platform with 1-DOF configuration. In each experiment, we try to maintain the same magnitude and frequency (about 0.5 rad and 0.5 Hz) of the actual position to have a fair comparison. (a) NAC. (b) TDA-based admittance control. (c) ESO-based admittance control. (d) Proposed method.

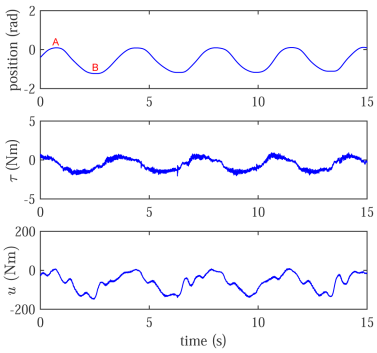

Fig. 13. Experimental results for workload analysis on the platform with 1-DOF configuration.

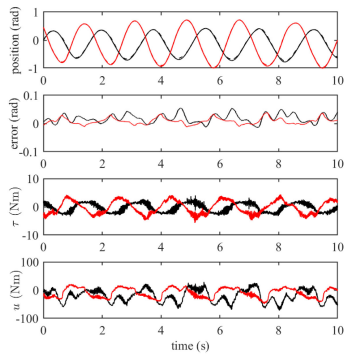

Fig. 14. Experimental results on the platform with 2-DOF configuration. Black: Joint 1. Red: Joint 2. Solid line in the first subfigure: Desired position. Dashed line in the first subfigure: Actual position.

the robot encounters with, cannot be fully characterized by this model. Nevertheless, choosing a suitable estimation model requires prior knowledge and is not easy in practice. On the contrary, the proposed method does not need to prescribe a disturbance model, instead it directly reduces the disturbance effect on the output over the full frequency range. Hence, the proposed method can work under a wider range of disturbance.

4) Workload Reduction for Load Lifting: This section will present how many workloads our method can reduce for load-lifting task by augmenting the admittance at the interactive port on the platform with 1-DOF configuration. The desired admittance is set to be $m_d = 0.1m$, $b_d = 0.1b$, and $k_d = 0.1k$. The human drives the robot link rotating from the vertical (i.e.,

0 rad) to the horizontal position (i.e., $-\frac{\pi}{2}$ rad). The results are shown in Fig. 13, where A (i.e., 0.0911 rad) is near the vertical position, while B (i.e., -1.2293 rad) is near the horizontal position. We take the data between A and B to analyze the energy exerted by the human and robot.

The work done by the human arm and robot can be calculated as

$$W_h = \int_{t_A}^{t_B} \tau\dot{\theta}\mathrm{d}t = 1.8376 \text{ J},\ W_r = \int_{t_A}^{t_B} u\dot{\theta}\mathrm{d}t = 113.7887 \text{ J}$$

where t_A and t_B are the times at A and B, respectively. Here, we neglect the kinematic energy and only consider the change of gravitational potential energy, which is calculated as

$$W_g = \tilde{m}_2 g l_2 \left[\sin(|\theta_B|) - \sin(|\theta_A|)\right] = 82.9307 \text{ J}$$

where $\tilde{m}_2 = 8.8$ kg is the load mass, g takes 9.8 $\mathrm{m/s^2}$, $l_2 = 0.91$ m is the link length, and θ_A and θ_B are the joint angles at A and B, respectively.

One can find that the work done by the human arm is smaller than 2% and 3% of the robot's and the load's, respectively. The human only needs about $1 \sim 2$-N·m torque to lift up the heavy load. Hence, the proposed method is effective in augmenting human strength by reducing the interactive impedance.

5) Impedance Reduction on the Platform With 2-DOF Configuration: To demonstrate the effectiveness of the proposed method, we also conduct experiments on the platform with 2-DOF configuration mounted with the heavy load. The human hands can drive the two joints to rotate simultaneously. The desired admittance parameters for the two joints are all set as $m_d = 0.15m$, $b_d = 0.15b$, and $k_d = 0.15k$. The results are shown in Fig. 14. The maximum admittance errors for the two joints are 0.0545 and 0.0382 rad, respectively, while the maximum interaction torques are 4.0274 and 5.6985 N·m, respectively. It should be noted that the maximum actual positions for the 2-DOF configuration increase to 0.7369 and 0.9545 rad, respectively, which inevitably results in relatively larger interaction torques. Nevertheless, compared with the load torque, the torque exerted by the human arm is much smaller.

VI. Conclusion

In this article, a multi-objective complementary control framework with decoupled design freedoms for passive and robust admittance control in human strength augmentation was proposed. We showed that PAC is achievable by a FI feedback controller, which acts as the nominal controller under ideal condition. To attenuate the disturbance/uncertainty, a robust regulator was added into the system without interference with the design of the nominal controller. The final controller was designed with three units: 1) a standard LQG for state estimation and noise rejection; 2) a feedforward controller, which, together with the LQG, renders the nominally passive and accurate admittance performance; and 3) a robust regulator for disturbance/uncertainty attenuation. In the simulation, the proposed controller was demonstrated with its ability of passive and accurate admittance rendering. The robust regulator can effectively handle the external disturbance without compromising the nominal admittance performance. During the experiments, precise admittance matching and passive interaction were achieved by our method regardless of the existence of the unknown load. We believe our methods can also be applied in many other admittance-controlled applications of physical human–robot interaction. In future work, the focus will be on addressing the nonlinear effect and model uncertainty in a more efficient way based on the proposed method.

References

[1] A. B. Zoss, H. Kazerooni, and A. Chu, "Biomechanical design of the berkeley lower extremity exoskeleton (BLEEX)," *IEEE/ASME Trans. Mechatronics*, vol. 11, no. 2, pp. 1330–1334, Apr. 2006.

[2] M. J. Kim *et al.*, "A passivity-based nonlinear admittance control with application to powered upper-limb control under unknown environmental interactions," *IEEE/ASME Trans. Mechatronics*, vol. 24, no. 4, pp. 1330–1334, Aug. 2019.

[3] B. He, G. C. Thomas, N. Paine, and L. Sentis, "Modeling and loop shaping of single-joint amplification exoskeleton with contact sensing and series elastic actuation," in *Proc. Amer. Control Conf.*, 2019, pp. 1330–1334.

[4] D. Buongiorno, D. Chiaradia, S. Marcheschi, M. Solazzi, and A. Frisoli, "Multi-DOFs exoskeleton-based bilateral teleoperation with the time-domain passivity approach," *Robotica*, vol. 37, no. 9, pp. 1330–1334, 2019.

[5] S. Y. Lee, K. Y. Lee, S. H. Lee, J. W. Kim, and C. S. Han, "Human–robot cooperation control for installing heavy construction materials," *Auton. Robots*, vol. 22, no. 3, pp. 1330–1334, 2007.

[6] L. Roveda, S. Haghshenas, M. Caimmi, N. Pedrocchi, and L. M. Tosatti, "Assisting operators in heavy industrial tasks: On the design of an optimized cooperative impedance fuzzy-controller with embedded safety rules," *Front. Robot. AI*, vol. 6, 2019, Art. no. 75.

[7] P. G. Griffiths, R. B. Gillespie, and J. S. Freudenberg, "A fundamental linear systems conflict between performance and passivity in haptic rendering," *IEEE Trans. Robot.*, vol. 27, no. 1, pp. 1330–1334, Feb. 2011.

[8] I. M. Horowitz, *Synthesis of Feedback Systems*. Cambridge, MA, USA: Academic Press, 1963.

[9] W. S. Newman, "Stability and performance limits of interaction controllers," *J. Dyn. Syst., Meas., Control*, vol. 114, no. 4, pp. 1330–1334, 1992.

[10] K. Zhou and J. C. Doyle, *Essentials of Robust Control*, vol. 104. Upper Saddle River, NJ, USA: Prentice Hall, 1998.

[11] J. E. Colgate and N. Hogan, "Robust control of dynamically interacting systems," *Int. J. Control*, vol. 48, no. 1, pp. 1330–1334, 1988.

[12] W. S. Newman and Y. Zhang, "Stable interaction control and coulomb friction compensation using natural admittance control," *J. Robot. Syst.*, vol. 11, no. 1, pp. 1330–1334, 1994.

[13] G. Aguirre-Ollinger, J. E. Colgate, M. A. Peshkin, and A. Goswami, "Design of an active one-degree-of-freedom lower-limb exoskeleton with inertia compensation," *Int. J. Robot. Res.*, vol. 30, no. 4, pp. 1330–1334, 2011.

[14] A. Q. Keemink, H. van der Kooij, and A. H. Stienen, "Admittance control for physical human–robot interaction," *Int. J. Robot. Res.*, vol. 37, no. 11, pp. 1330–1334, 2018.

[15] R. J. Adams and B. Hannaford, "Stable haptic interaction with virtual environments," *IEEE Trans. Robot. Autom.*, vol. 15, no. 3, pp. 1330–1334, Jun. 1999.

[16] K. Hashtrudi-Zaad and S. E. Salcudean, "Analysis of control architectures for teleoperation systems with impedance/admittance master and slave manipulators," *Int. J. Robot. Res.*, vol. 20, no. 6, pp. 1330–1334, 2001.

[17] B. Willaert, B. Corteville, D. Reynaerts, H. van Brussel, and E. B. V. Poorten, "Bounded environment passivity of the classical position-force teleoperation controller," in *Proc. IEEE/RSJ Int. Conf. Intell. Robots Syst.*, 2009, pp. 1330–1334.

[18] H. Vallery, J. Veneman, E. Van Asseldonk, R. Ekkelenkamp, M. Buss, and H. van der Kooij, "Compliant actuation of rehabilitation robots," *IEEE Robot. Autom. Mag.*, vol. 15, no. 3, pp. 1330–1334, Sep. 2008.

[19] F. Sergi and M. K. O'Malley, "On the stability and accuracy of high stiffness rendering in non-backdrivable actuators through series elasticity," *Mechatronics*, vol. 26, pp. 1330–1334, 2015.

[20] A. Calanca, R. Muradore, and P. Fiorini, "Impedance control of series elastic actuators: Passivity and acceleration-based control," *Mechatronics*, vol. 47, pp. 1330–1334, 2017.

[21] F. E. Tosun and V. Patoglu, "Necessary and sufficient conditions for the passivity of impedance rendering with velocity-sourced series elastic actuation," *IEEE Trans. Robot.*, vol. 36, no. 3, pp. 1330–1334, Jun. 2020.

[22] B. Hannaford and J.-H. Ryu, "Time-domain passivity control of haptic interfaces," *IEEE Trans. Robot. Autom.*, vol. 18, no. 1, pp. 1330–1334, Feb. 2002.
[23] S. F. Atashzar, M. Shahbazi, M. Tavakoli, and R. V. Patel, "A passivity-based approach for stable patient– robot interaction in haptics-enabled rehabilitation systems: Modulated time-domain passivity control," *IEEE Trans. Control Syst. Technol.*, vol. 25, no. 3, pp. 1330–1334, May 2017.
[24] F. Ferraguti *et al.*, "An energy tank-based interactive control architecture for autonomous and teleoperated robotic surgery," *IEEE Trans. Robot.*, vol. 31, no. 5, pp. 1330–1334, Oct. 2015.
[25] C. Ott, A. Albu-Schaffer, A. Kugi, and G. Hirzinger, "On the passivity-based impedance control of flexible joint robots," *IEEE Trans. Robot.*, vol. 24, no. 2, pp. 1330–1334, Apr. 2008.
[26] Q. Zhang and G. Liu, "Precise control of elastic joint robot using an interconnection and damping assignment passivity-based approach," *IEEE/ASME Trans. Mechatronics*, vol. 21, no. 6, pp. 1330–1334, Dec. 2016.
[27] T. Zhang and J. Xia, "Interconnection and damping assignment passivity-based impedance control of a compliant assistive robot for physical human–robot interactions," *IEEE Robot. Autom. Lett.*, vol. 4, no. 2, pp. 1330–1334, Apr. 2019.
[28] Z. Li, B. Huang, Z. Ye, M. Deng, and C. Yang, "Physical human–robot interaction of a robotic exoskeleton by admittance control," *IEEE Trans. Ind. Electron.*, vol. 65, no. 12, pp. 1330–1334, Dec. 2018.
[29] Y. Tu *et al.*, "An adaptive sliding mode variable admittance control method for lower limb rehabilitation exoskeleton robot," *Appl. Sci.*, vol. 10, no. 7, 2020, Art. no. 2536.
[30] I. Ranatunga,F. L. Lewis, D. O. Popa, and S. M. Tousif, "Adaptive admittance control for human-robot interaction using model reference design and adaptive inverse filtering," *IEEE Trans. Control Syst. Technol.*, vol. 25, no. 1, pp. 1330–1334, Jan. 2017.
[31] M. Dohring and W. Newman, "Admittance enhancement in force feedback of dynamic systems," in *Proc. IEEE Int. Conf. Robot. Autom.*, 2002, pp. 1330–1334.
[32] M. Kristalny and J. H. Cho, "Circumventing conceptual flaws in classical interaction control strategies," in *Proc. IEEE/RSJ Int. Conf. Intell. Robots Syst.*, 2021, pp. 1330–1334.
[33] D. Youla, J. Bongiorno, and H. Jabr, "Modern Wiener–Hopf design of optimal controllers part I: The single-input–output case," *IEEE Trans. Autom. Control*, vol. 21, no. 1, pp. 1330–1334, Feb. 1976.
[34] D. Youla and J. Bongiorno, "A feedback theory of two-degree-of-freedom optimal Wiener–Hopf design," *IEEE Trans. Autom. Control*, vol. 30, no. 7, pp. 1330–1334, Jul. 1985.
[35] K. Zhou and Z. Ren, "A new controller architecture for high performance, robust, and fault-tolerant control," *IEEE Trans. Autom. Control*, vol. 46, no. 10, pp. 1330–1334, Oct. 2001.
[36] X. Chen, K. Zhou, and Y. Tan, "Revisit of LQG control—A new paradigm with recovered robustness," in *Proc. IEEE 58th Conf. Decis. Control*, 2019, pp. 1330–1334.
[37] V. Kucera, *Discrete Linear Control: The Polynomial Equation Approach*. Hoboken, NJ, USA: Wiley, 1980.
[38] P. Apkarian and D. Noll, "Nonsmooth optimization for multiband frequency domain control design," *Automatica*, vol. 43, no. 4, pp. 1330–1334, 2007.
[39] S. Li, J. Yang, W. H. Chen, and X. Chen, *Disturbance Observer-Based Control: Methods and Applications*. Boca Raton, FL, USA: CRC press, 2016.

Wulin Zou received the B.E. degree in automation and the M.S. degree in control science and engineering from Nankai University, Tianjin, China, in 2015 and 2018, respectively. He is currently working toward the Ph.D. degree in electronic and computer engineering with the Department of Electronic and Computer Engineering, Hong Kong University of Science and Technology, Hong Kong, China.

His research interests include exoskeleton robots, compliance control, and robust position/force control.

Xiang Chen (Member, IEEE) received the M.Sc. and Ph.D. degrees in systems and control from Louisiana State University, Baton Rouge, LA, USA, in 1996 and 1998, respectively.

Since 2000, he has been with the Department of Electrical and Computer Engineering, University of Windsor, Windsor, ON, Canada, where he is currently a Professor. His research interests include robust control, vision sensor networks, vision-based control systems, networked control systems, and industrial applications of control theory.

Prof. Chen is a Senior Editor of the IEEE/ASME TRANSACTIONS ON MECHATRONICS and an Associate Editor for the *SIAM Journal on Control and Optimization*.

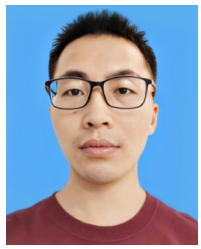

Shilei Li received the B.E. degree in detection guidance and control technology and the M.S. degree in control engineering from the Harbin Institute of Technology, Harbin, China, in 2015 and 2018, respectively. He is currently working toward the Ph.D. degree in electronic and computer engineering with the Department of Electronic and Computer Engineering, Hong Kong University of Science and Technology, Hong Kong, China.

His research interests include sensor fusion, synchronization control, and human–robot interaction.

Pu Duan received the B.E. degree in mechanical engineering from the University of Science and Technology Beijing, Beijing, China, in 2008, the M.S. degree in advanced mechanical engineering from Imperial College London, U.K., in 2009, and the Ph.D. degree in armament science and technology from the Beijing Institute of Technology, Beijing, China, in 2018.

He is currently a Research Engineer with Xeno Dynamics, Company, Ltd, Shenzhen, Guangdong, China. His research focuses on sensing, control, and system design of human-centered robots.

Ningbo Yu (Member, IEEE) received the B.E. degree in precision engineering from Tianjin University, Tianjin, China, in 2003, the M.Phil. degree in electrical and electronic engineering from the Hong Kong University of Science and Technology, Hong Kong, China, in 2005, and the Ph.D. degree from ETH Zurich, Zurich, Switzerland, in 2011.

He is currently a Professor with the Institute of Robotics and Automatic Information Systems, Nankai University, Tianjin, China. His research interests include assistive and rehabilitation robotics and physical human–robot interaction and coordination.

Ling Shi (Senior Member, IEEE) received the B.E. degree in electrical and electronic engineering from the Hong Kong University of Science and Technology, Kowloon, Hong Kong, in 2002, and the Ph.D. degree in control and dynamical systems from the California Institute of Technology, Pasadena, CA, USA, in 2008.

He is currently a Professor with the Department of Electronic and Computer Engineering and the Associate Director of Robotics Institute, Hong Kong University of Science and Technology. His research interests include cyber-physical systems security, networked control systems, sensor scheduling, event-based state estimation, and exoskeleton robots.

Prof. Shi was an Editorial Board Member of the European Control Conference (2013–2016). He was a Subject Editor of the *International Journal of Robust and Nonlinear Control* (2015–2017) and an Associate Editor for the IEEE TRANSACTIONS ON CONTROL OF NETWORK SYSTEMS (2016–2020), *IEEE Control Systems Letters* (2017–2020), and for a special issue on Secure Control of Cyber Physical Systems in IEEE TRANSACTIONS ON CONTROL OF NETWORK SYSTEMS (2015–2017). He was the General Chair of the 23rd International Symposium on Mathematical Theory of Networks and Systems (MTNS 2018). He is a member of the Young Scientists Class 2020 of the World Economic Forum.